Heavy flavour production at LHCb

Marcello Rotondo[*][†]

INFN Laboratori Nazionali di Frascati, Frascati, Italy

E-mail: marcello.rotondo@lnfn.infn.it

The measurements of heavy flavour production in pp collisions provide crucial inputs to study both perturbative and non-perturbative quantum chromodynamics. Moreover these measurements allow to improve the precision on the study of heavy hadron decays. LHCb has a large program of studies of heavy flavour production and it has, compared with other experiments at the LHC, the unique feature to cover the very forward region. In this paper the most recent results on the quarkonia production and fragmentation fractions for various kinds of heavy hadrons are presented.

---

[*]Speaker.

[†]On behalf of the LHCb collaboration

PoS(Beauty2019)025

1. Introduction

The detailed study of heavy-flavour production provides a crucial testing ground for both perturbative and non-perturbative aspects of quantum chromodynamics (QCD) calculations. Various models that predict the kinematics of heavy hadrons in a wide range of transverse momentum and pseudorapidy are available. Even if these models predict many features of the production, there are still many aspects of the mechanisms that require further studies from both the experimental and theoretical side.

In addition to the understanding of the underlying mechanism for heavy hadron formation, precise knowledge of the properties and kinematics of the heavy hadrons are crucial for the precise studies of their decays. For example the knowledge of the polarization of the Λ_b in production is important for pentaquark analysis using $\Lambda_b \to J/\psi K^- p$ decays [1].

The LHCb detector [2, 3], with its high momentum resolution, great particle identification capability and flexible trigger strategy, is perfectly suited to study heavy flavour production features. In this paper the following recent LHCb results on heavy hadron production are summarized:

- $\psi(2S)$ production cross-sections [4],

- $\eta_c(1S)$ production cross-section [5] ,

- Ξ_{cc}^{++} production [6],

- B_s and Λ_b production fractions [7] ,

- B_c production fractions [8] ,

- Ξ_b^- production rate [9].

The datasets and the integrated luminosity used to obtain these results are reported in Table 1.

2. Heavy quarkonium

The study of heavy quarkonium production plays a central role because it helps in understanding how quarks combine into bound states. Heavy quarkonium production involves two steps: the production of a heavy quark pair, $q\bar{q}$, and its following hadronization in a specific quarkonium state.

Table 1: List of the analyses included in this paper with the datasets and the corresponding integrated luminosity used.

Reference		7 *TeV*	8 *TeV*	13 *TeV*
[4]	$\psi(2S)$ production cross-sections	614 pb^{-1}	-	275 pb^{-1}
[5]	$\eta_c(1S)$ production cross-section	-	-	2.0 fb^{-1}
[6]	Ξ_{cc}^{++} production	-	-	1.7 fb^{-1}
[7]	B_s and Λ_b production fractions	-	-	1.67 fb^{-1}
[8]	B_c production fractions	1.0 fb^{-1}	-	1.7 fb^{-1}
[9]	Ξ_b^- production rate	1.0 fb^{-1}	1.0 fb^{-1}	1.6 fb^{-1}

In general the first step can be computed with perturbative QCD, while the hadronization is merely non-perturbative and must be determined using experimental results. For this reason the underlying physics process of heavy quarkonium can probe both the perturbative and non-perturbative regime of QCD.

The nonrelativistic QCD approach [10] (NRQCD) predicts many features of quarkonium production and it is widely applicable. In this effective theory, intermediate $q\bar{q}$ states with all possible colour and spin quantum numbers, have probabilities to fragment into a specific quarkonium. The transition probabilities are described by long distance matrix elements (LDME) that must be determined from data. These matrix elements are assumed to be universal and can be applied to different quarkonium states. Despite the success of NRQCD in the description of quarkonium cross sections, it predicts a large transverse polarization of the J/ψ that is not supported by experimental results. In the following, recent studies of the production of the $\psi(2S)$ and η_c states are reported.

## 2.1 $\psi(2S)$ production at $\sqrt{s} = 7$ and $13\ TeV$

In high energy pp collisions, quarkonium states are produced from three different sources: directly from the hard collision, through feed-down of higher excited states or through the weak decays of b-hadrons. While the latter contribution can be disentangled exploiting the large lifetime of the b-hadrons, the contamination from the decays of excited states makes the comparison with the predictions complicated. For example the prompt J/ψ production is affected by large feed-down from radiative decays of χ_c states. Instead the feed-down to the $\psi(2S)$ state is almost negligible so theoretical predictions can be directly compared with the experimental results.

In this analysis the $\psi(2S)$ production cross section is studied for both the prompt contribution, *prompt $\psi(2S)$*, and from b-hadron decays, *$\psi(2S)$-from-b*. The $\psi(2S)$ are reconstructed through the $\psi(2S) \to \mu^+\mu^-$ decay mode. The kinematic region in rapidity and transverse momentum analysed is $2.0 < y < 4.5$, and $3.5 < p_T < 14\ GeV/c$ at 7 TeV, and $2 < p_T < 14\ GeV/c$ at 13 TeV. The variable most useful to separate prompt $\psi(2S)$ and $\psi(2S)$ from b-decays is the *pseudo decay time* t_z, defined as

$$t_z = \left(z_{\psi(2S)} - z_{PV}\right) \cdot \frac{M_{\psi(2S)}}{p_z}, \tag{2.1}$$

where $z_{\psi(2S)}$ and z_{PV} are the z-coordinates of the reconstructed $\psi(2S)$ decay vertex and the associated Primary Vertex (PV), respectively; p_z is the z-component of the measured $\psi(2S)$ momentum, and $M_{\psi(2S)}$ is the $\psi(2S)$ mass.

The main result of the analysis is the differential cross section $d^2\sigma/dy dp_T$ separately for the prompt $\psi(2S)$ and $\psi(2S)$-from-b samples. The differential cross section in a given (y, p_T) bin, is obtained from the $\psi(2S)$ yields, corrected for the total efficiency to reconstruct a $\psi(2S)$, the integrated luminosity and the $\psi(2S) \to \mu^+\mu^-$ branching fraction. The yields of prompt $\psi(2S)$ and $\psi(2S)$ from b-decay candidates are determined in each (y, p_T) bin by a two dimensional fit to the distribution of the invariant mass $m_{\mu^+\mu^-}$ and the pseudo-proper time t_z. In Fig. 1 is shown an example of the $m_{\mu^+\mu^-}$ and t_z distributions in a single bin of y and p_T. The distribution of t_z is described by a δ function for the prompt $\psi(2S)$ and an exponential for the $\psi(2S)$-from-b, both convolved with an appropriate resolution function. The background is described by an empirical function whose shape is guided by the events in the $m_{\mu^+\mu^-}$ side bands.
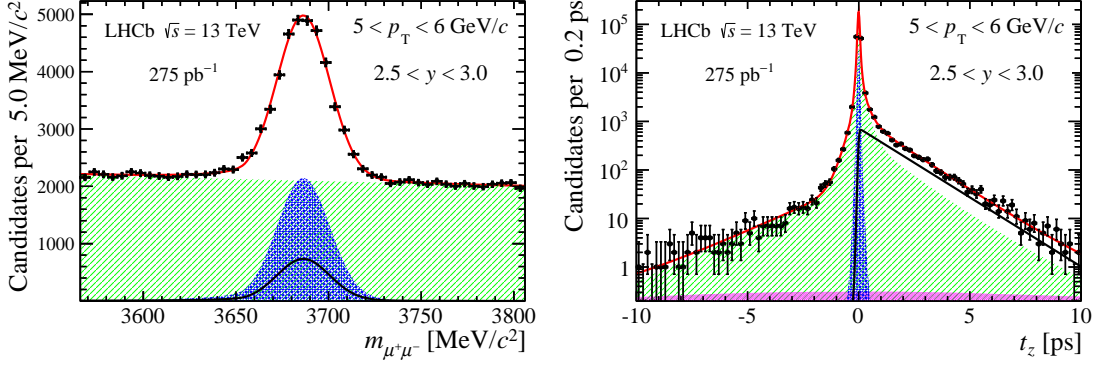
Figure 1: Distributions of the invariant mass $m_{\mu^+\mu^-}$ (left) and the pseudo decay time t_z (right) of selected $\psi(2S)$ candidates in a bin of y and p_T in the 13 TeV data sample. Projections of the two-dimensional fit result are also shown.

The main result is the double-differential production cross-section $d^2\sigma/dydp_T$ for prompt $\psi(2S)$ and $\psi(2S)$-from-b, assuming no polarisation of the $\psi(2S)$. The distributions of $d\sigma/dp_T$, obtained integrating the double-differential cross section over y, are shown in Fig.2 for both data at 7 TeV and 13 TeV. The predictions for the prompt $\psi(2S)$ production based on the NRQCD [10], and for the $\psi(2S)$-from-b obtained with the Fixed Order plus Next-to-Leading Logarithm (FONLL) calculations [11], are superimposed on the experimental results. The NRQCD calculation shows reasonable agreement with the data for $p_T > 7$ GeV/c, while predictions are omitted at lower momentum where they are not reliable. The FONLL calculation agrees very well with the measurements in the full range considered. The same good agreement is present for the y distributions obtained by integrating over p_T.
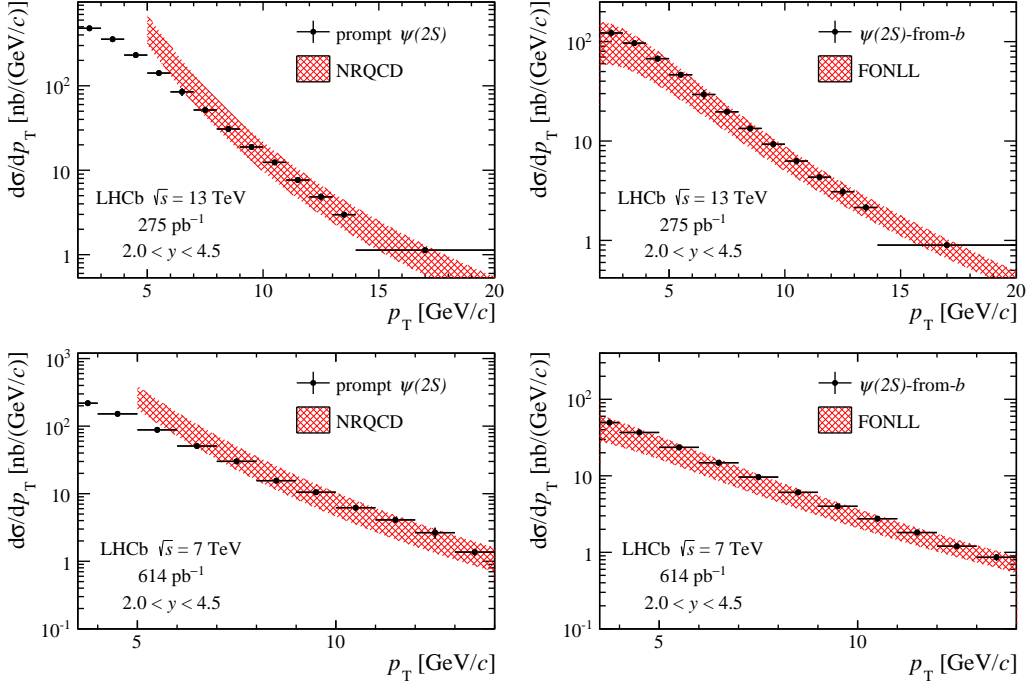
The production cross sections of $\psi(2S)$ are compared with those of the J/ψ mesons measured by LHCb at $\sqrt{s} = 13$ TeV [12]. These ratios of cross sections, $R(\psi(2S)/J/\psi)$, increase with p_T for both prompt and from-b $\psi(2S)$. The FONLL calculation predicts very well the ratio $R(\psi(2S)/J/\psi)$ for $\psi(2S)$ and J/ψ from b-hadron decays, while the NRQCD shows only reasonable agreement for prompt $\psi(2S)$ and J/ψ.

The production cross-sections of the $\psi(2S)$ are also compared for the 13 TeV and 7 TeV samples. The ratio $R_{13/7}$ is about 1.5 for prompt $\psi(2S)$ and it increases slightly with the p_T; this behaviour is well predicted by the NRQCD model. For the $\psi(2S)$-from-b the measured ratio $R_{13/7}$ is well predicted by the FONLL calculation.

2.2 $\eta_c(1S)$ production at $\sqrt{s} = 13$ TeV

The NRQCD framework allows to simultaneously treat the J/ψ ($J^{CP} = 1^{--}$) and η_c ($J^{CP} = 0^{-+}$) production imposing relations between their LDME, under the assumption of factorization and heavy-quark spin symmetry. The simultaneous study of η_c and J/ψ prompt production and production from b-hadron decays, provides an important test of the basic NRQCD assumptions.

In this analysis the differential production cross-section of the η_c is measured in the region $6.5 < p_T < 14.0$ GeV/c and $2.0 < y < 4.5$. The measurement is performed relative to that of the J/ψ meson, in four bins of p_T. Both the η_c and the J/ψ are reconstructed in the $p\bar{p}$ decay mode.

Figure 2: Differential production cross-sections as functions of p_T for the 13 *TeV* (top) and the 7 *TeV* sample (bottom). The figures on the left are for prompt $\psi(2S)$ and the results compared with the NRQCD [10] calculations; the figures on the right are for $\psi(2S)$-from-b and the results are compared with the FONLL calculations [11].

The actual measurements are the ratios of cross sections, $(d\sigma_{\eta_c}/dp_T)/(d\sigma_{J/Psi}/dp_T)$, separately for prompt η_c and η_c-from-b decays. Because the $p\bar{p}$ pairs from η_c and J/ψ decays have comparable kinematics, they have similar reconstruction, trigger and selection efficiencies. The prompt η_c and J/ψ are distinguished from the b-hadron decays using the pseudo-proper time t_z defined as in Eq.2.1. A prompt-enriched sample is defined requiring $t_z < 80\ fs$, while a b-hadron enriched sample is selected by $t_z > 80\ fs$. The small cross-feed between the two samples is evaluated with simulation.

The J/ψ yields and the ratio of η_c and J/ψ are extracted from a simultaneous fit to the $p\bar{p}$ invariant mass distribution in the prompt-enriched and b-hadron enriched samples. The $p\bar{p}$ invariant mass distributions are shown in Fig.3 with the result of the fits, integrated over p_T, superimposed.

The ratio of prompt production of η_c and J/ψ as a function of p_T is shown in Fig.4 (left). After integration over p_T, the relative prompt production cross section $\sigma_{\eta_c}/\sigma_{J/\psi}$ is $1.69 \pm 0.15_{stat} \pm 0.10_{syst} \pm 0.18_{BF}$ where the last uncertainty is due to the $J/\psi \to p\bar{p}$ and $\eta_c \to p\bar{p}$ branching fractions. This measurement supports the conclusions of the LHCb measurement at $\sqrt{s} = 7$ and 8 *TeV*, reported in [13], that η_c production is enhanced compared to that of the J/ψ. Using $\sigma_{J\psi} = 0.749 \pm 0.047\ \mu b$ for the prompt J/ψ production [12], the prompt η_c production cross section in the considered fiducial region is

$$\sigma_{\eta_c}^{prompt} = 1.26 \pm 0.11_{stat} \pm 0.08_{syst} \pm 0.14_{\sigma_{J/\psi}}\ \mu b,$$

which is in good agreement with the *colour-singlet* model prediction, $1.56^{+0.83+0.38}_{-0.49-0.17}\ \mu b$ [14]. The
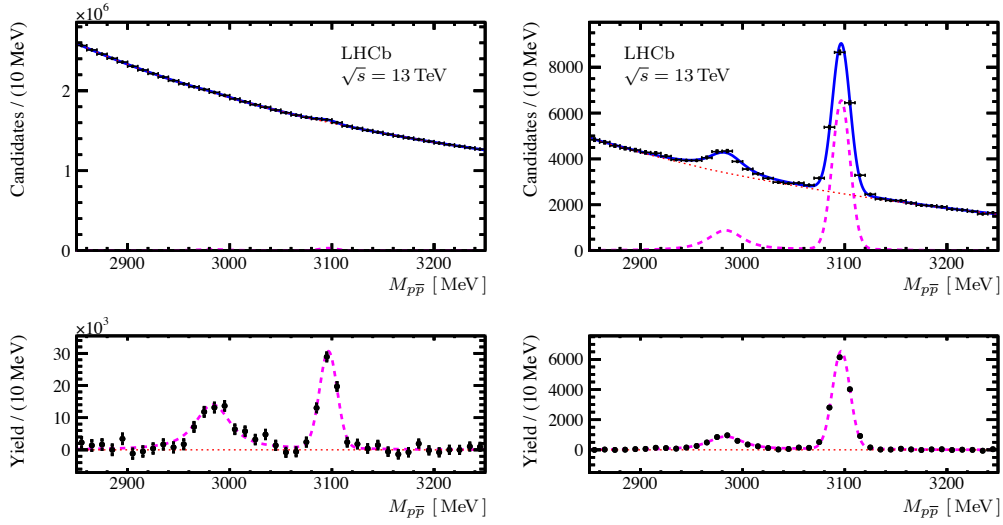
Figure 3: Invariant-mass distribution of the *pp̄* candidates for (top left) prompt-enriched with $t_z < 80\,fs$ and (top right) *b*-hadron enriched with $t_z > 80\,fs$ samples. Signal distributions with the background components from the fit subtracted are shown on the bottom plots for the two samples.
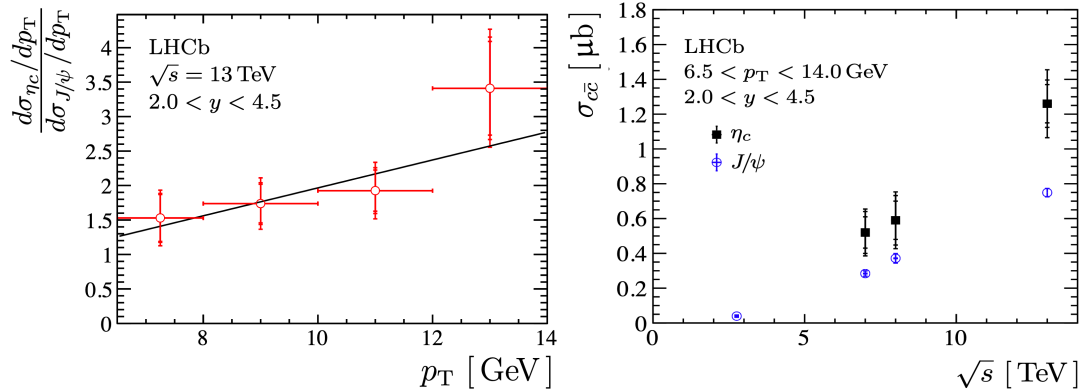
Figure 4: (Left) Ratios of η_c to J/ψ differential production cross-sections for prompt production. The result of a fit with a linear function is overlaid. (Right) Absolute η_c (black rectangles) and J/ψ (blue circles) prompt production cross-sections.

LHCb result confirms the theoretical analyses [15, 16, 17] that follow the LHCb first measurements at $\sqrt{s} = 7$ and $8\,TeV$. It is worth mentioning that these theoretical analyses do not predict the slope observed in Fig.4(left) that shows p_T dependent differences between the J/ψ and η_c production cross sections. Further studies are needed, for example extending the p_T region analysed.

The η_c production cross-section dependence on $\sqrt{s}$ is shown in Fig.4 (right) with the results on the prompt J/ψ cross section superimposed for reference. The relative η_c production rate from *b*-hadron decays is measured to be $\mathscr{B}(b \to \eta_c X)/\mathscr{B}(b \to J/\psi X) = 0.48_{stat} \pm 0.03_{syst} \pm 0.05_{BF}$, which is the most precise measurement of the inclusive $b \to \eta_c X$ branching ratio and is in good agreement with a previous LHCb measurement [13].

3. Open charm and beauty

The measurements of branching fractions of specific decay channels of *b*-hadrons are often needed to make quantitative comparisons with theoretical predictions. The absolute branching fraction measurements at hadron colliders are difficult without external inputs. In general the branching fraction of a decay channel is measured relative to a channel with similar decay topology, that often is a decay of a B^0 or B^- meson whose absolute branching ratio is known well from B-factories. These measurements require the knowledge of the *production fraction* of any specific heavy hadron H_b, called f_{H_b}, which is the probability that a *b*-quark fragments into the H_b hadron. For example the probabilities that a *b*-quark hadronize into a B^0, B_s^0, Λ_b^0 or a B_c^+, are f_d, f_s, f_{Λ_b} and f_c respectively.

3.1 Ξ_{cc} production at $\sqrt{s} = 13\ TeV$

Since the observation of the Ξ_{cc}^{++} baryon into the $\Lambda_c^+ K^- \pi^+ \pi^+$ decay mode [18], many studies have been published to study its property: the lifetime has been measured and found consistent with a weak decay, the decay mode $\Xi_{cc}^{++} \rightarrow \Xi_c^+ \pi^+$ has been observed, and a search for the single charmed decay $\Xi_{cc}^{++} \rightarrow D^+ p K^- \pi^+$ has found no signal. The data sample corresponding to 1.5 fb^{-1} taken at $\sqrt{s} = 13\ TeV$ is used to study Ξ_{cc}^{++} production. In this measurement the Ξ_{cc}^{++} production cross section times its branching fraction into $\Lambda_c^+ K^- \pi^+ \pi^+$, $\sigma(\Xi_{cc}^{++}) \times \mathscr{B}(\Xi_{cc}^{++} \rightarrow \Lambda_c^+ K^- \pi^+ \pi^+)$, is measured relative to the Λ_c^+ prompt production cross section, $\sigma(\Lambda_c^+)$, in the kinematic region $4 < p_T < 15\ GeV/c$ and $2.0 < y < 4.5$.

The Λ_c^+, reconstructed in the $p K^- \pi^+$ decay mode, is required to form a good vertex well-separated from the PV. The additional tracks have to be well identified, and have to form a vertex with the Λ_c^+ candidate. The formed Ξ_{cc}^{++} candidates are required to have a p_T greater than 4 GeV and to originate from a PV. The combinatorial background is suppressed using a multivariate classifier using vertex and kinematic information of the Ξ_{cc}^{++} decay products.

After all the selection requirements, the distribution of the invariant mass of Ξ_{cc}^{++} candidates is shown in Fig. 5 for two different trigger lines used.
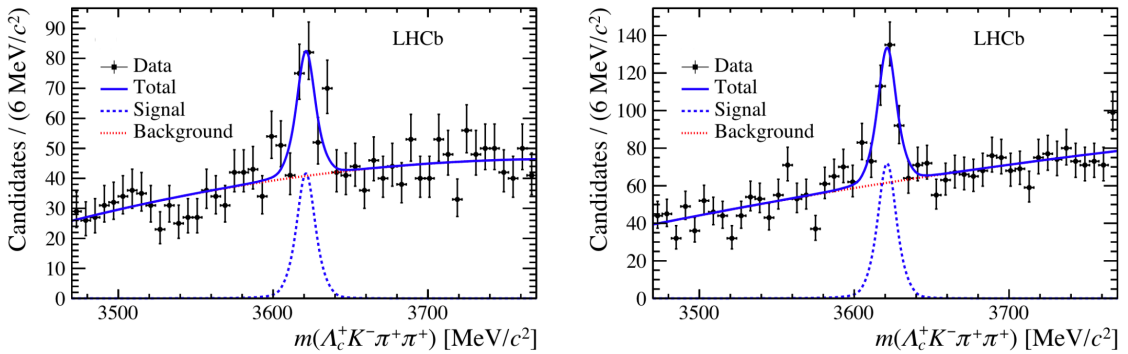
Figure 5: Invariant-mass distributions of Ξ_{cc}^{++} candidates (left) triggered by particles belonging to the signal and (right) triggered exclusively by particles unrelated to the signal.

The prompt Λ_c^+ production sample requires particular care, because of the contamination from Λ_c^+'s from *b*-hadron decays. A powerful variable useful to disentangle these two source of Λ_c^+ is

the $\Delta\chi_{IP}$ which is defined as the difference in the χ^2 of the PV fit with and without the particles from the Λ_c^+ decay candidate. The prompt Λ_c^+ are characterized by lower values of $\Delta\chi^2_{IP}$, while Λ_c^+ from other processes have larger $\Delta\chi_{IP}$ values. The efficiency to reconstruct Ξ_{cc}^{++}'s depends strongly on Ξ_{cc}^{++} lifetime, and assuming the measured central value [19], the resulting Ξ_{cc}^{++} production cross section ratio is

$$\frac{\sigma(\Xi_{cc}^{++}) \times \mathscr{B}(\Xi_{cc}^{++} \to \Lambda_c^+ K^- \pi^+ \pi^-)}{\sigma(\Lambda_c^+)} = (2.22 \pm 0.27_{stat} \pm 0.29_{syst}) \times 10^{-4}.$$

This is the first measurement of the production of a doubly charmed baryon in pp collisions and gives important input to improve our understanding on its production mechanism.

3.2 Λ_b and B_s production at $\sqrt{s} = 13$ TeV

In this analysis the ratios $f_s/(f_u + f_d)$ and $f_{\Lambda_b^0}/(f_u + f_d)$ are extracted in the pseudorapidity range $2 < \eta < 5$ and transverse momentum range $4 < p_T < 25$ GeV/c using the data at $\sqrt{s} = 13$ TeV. Because these ratios can depend on p_T and η, a two-dimensional fit is performed in these variables.

This measurement exploits the theoretical prediction that the inclusive semileptonic decay widths, Γ_{SL}, are nearly the same for all b-hadrons with light or strange quark spectators [20]. As a consequence, the inclusive semileptonic branching ratio for the B_s and the Λ_b can be related to the precisely measured inclusive branching ratio $\mathscr{B}(B \to X_c \ell \nu_\ell) = \tau_B \Gamma_{SL}(B^0 + B^+) = (10.70 \pm 0.19)\%$ obtained at the B-Factories [21] through the following relations,

$$\begin{aligned}
\mathscr{B}(B_s \to X_c) &= \tau_s(\Gamma_{SL}(B) + \eta_s), \\
\mathscr{B}(\Lambda_b^0 \to X_c) &= \tau_{\Lambda_b}(\Gamma_{SL}(B) + \eta_{\Lambda_b}),
\end{aligned} \tag{3.1}$$

where τ_s and τ_{Λ_b} are the known lifetimes of B_s mesons and Λ_b baryons respectively, and η_s and η_{Λ_b} are small corrections to Γ_{SL} for B_s $(-1.0 \pm 0.5)\%$ and Λ_b $(+3.0 \pm 1.5)\%$ taken from [20]. The yields of the inclusive semileptonic decays of B^0 and B^+ are obtained as mixtures of decays $B^{0,+} \to D^0 \mu \nu X$ and $B^{0,+} \to D^+ \mu \nu X$, properly corrected for the selection and reconstruction efficiencies, and for the presence of a small component of $B \to D_s^{(*)+} K \mu \nu$ decays that do not give D^+ or D^0 in the final state. Similarly in the semileptonic decays of the B_s, mostly there is a D_s^+ in the final state. However there is also a non-negligible contribution that gives $D^0 K^+$ and $D^+ K^0$ pairs through excited D_s^{**} decays or from non-resonant DK pairs. These contributions are evaluated on data reconstructing explicitly $D^0 K^+ \mu \nu X$ events. Analogously, the Λ_b^0 decays semileptonically mainly with a Λ_c^+ in the final state, but there can also be $D^0 p$ or $D^+ n$ pairs produced. These are determined studying the $D^0 p \mu \nu X$ sample.

The different combinations analysed are $D^0 \mu \nu X$, $D^+ \mu \nu X$, $D_s^+ \mu \nu X$ and $\Lambda_c^+ \mu \nu X$. In all cases, well reconstructed $D^0 \to K\pi$, $D^+ \to K3\pi$, $D_s^+ \to K^+ K^- \pi^+$ and $\Lambda_c^+ \to p K^- \pi^+$, are required to form a good vertex well separated from the PV and not pointing to the PV itself. These hadrons are combined with a well identified μ with large p_T and coming from the same vertex.

The remaining component of B_s^0 decaying into DK must be added into the B_s yields and subtracted from the B^0 and B^+ yields. For the Λ_b the Dp component has to be added to the Λ_b^0 yields and subtracted from the fractions f_u and f_d. These signal components are evaluated adding
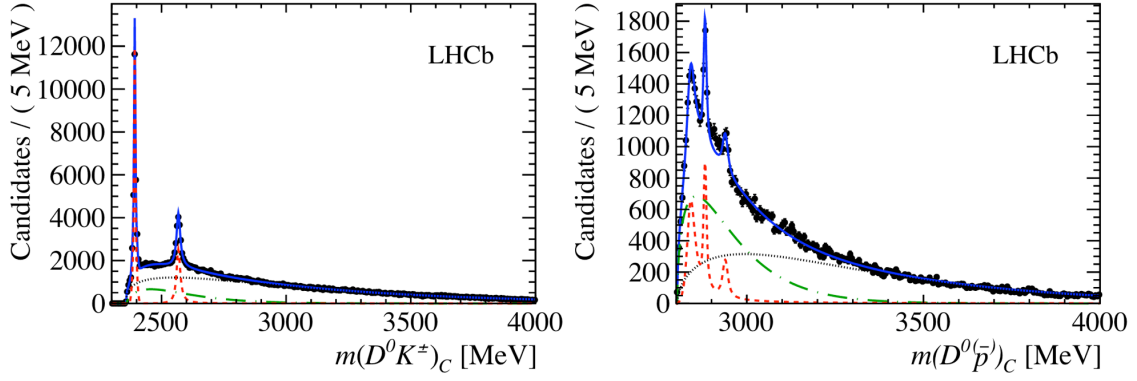
Figure 6: (Left) Projections of the two-dimensional fits onto the $m(D^0 K^+)$ for $D^0 K^+ \mu \nu X$ candidates (left). The two peaks correspond to the excited states $D_{s1}(2536)^+$ and $D_{s2}^*(2537)^+$. The non-resonant component (long-dashed, green) corresponds to about 50% of the $D^0 K^+$ sample. (Right) Projection of the $m(D^0 \bar{p})$ mass distribution for $D^0 p \mu \nu X$ candidates. The peaks due to $\Lambda_c^+(2860)$, $\Lambda_c^+(2880)$ and $\Lambda_c^+(2940)$ are visible. The non-resonant component is about 76% of the $D^0 p$ sample.

a further well identified K or a proton, to the $D^0 \mu \nu X$ samples. The resonant and non-resonant $B_s^0 \to D^0 K^+ \mu \nu X$ and $\Lambda_b^0 \to D^0 p \mu \nu X$ components are isolated from the large combinatorial background, through a two-dimensional fit to the distribution of the constrained DK invariant mass, defined as $m(DK)_C = m(DK) - m(D) + m(D)_{PDG}$ (analogously $m(Dp)_C$ mass, with an identified proton), and the $\Delta \chi_V$, which is defined as the difference between the vertex χ^2 formed by the added hadron track and the $D\mu$ system and the vertex χ^2 of the $D\mu$ system. The variable $\Delta \chi_V$ is smaller for events where the DK and Dp combinations come from resonant or non resonant $B_s \to D^0 K^+ \mu \nu_\mu$ and $\Lambda_b \to D^0 p \mu \nu_\mu$ semileptonic decays, and it takes a larger value if the additional track (kaon or proton) is not associated with the $D\mu$ vertex. The projection of these fits on $m(DK)$ and $m(Dp)$ distributions are shown in Fig.6 where, for both samples, the presence of excited states are clearly observed together with large non-resonant components. The unmeasured $D^+ K^0$ and $D^+ n$ are properly accounted using isospin conservation.

The production of the b-hadron H_b (B_s^0 or Λ_b^0) is evaluated in bins of η and $p_T(H_b)$. The pseudorapidity is determined by measuring the angle of the H_b hadron, whose direction is determined from the PV and the H_b decay vertex, with respect to the beam direction. Because of the presence of the neutrinos the $p_T(H_b)$ cannot be reconstructed directly. Instead $p_T(H_b)$ is inferred from the visible $H_c \mu$ systems applying a correction factor, *k-factor*, that is the ratio of the average reconstructed $p_T(H_c \mu)$ to the true $p_T(H_b)$, as a function of the invariant mass $m(H_c \mu)$. For illustration, the distribution of this ratio and the *k-factor* correction for the $B_c \to J/\psi \mu \nu$ decay mode is shown in Fig. 8 (right).

The distribution of $f_s/(f_u + f_d)$ and $f_{\Lambda_b}/(f_u + f_d)$ as a function of p_T are shown in Fig.7 (left). The distribution of $f_s/(f_u + f_d)$ is fitted with a linear function and the slope is significantly different from zero. The ratio $f_{\Lambda_b}/(f_u + f_d)$ shows instead a large p_T dependence, already observed in other LHCb analyses [22, 23]. The average values of the two ratios, obtained by integration over the
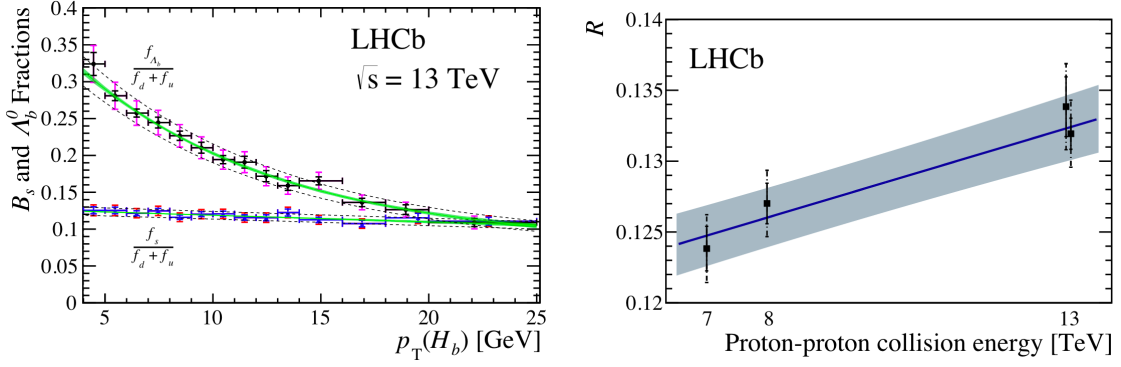
Figure 7: (Left) The B_s and Λ_b production fractions relative to $B^0 + B^+$, in bins of $p_T(H_b)$. (Right) Efficiency-corrected $B_s^0 \to J/\psi\phi$ and $B^+ \to J/\psi K^+$ yield ratios, R, at different pp collision energies as reported from LHCb in [24]. The ratio R is proportional to f_s/f_u.

kinematic range $4 < p_T < 25\ GeV/c$ and $2 < \eta < 5$, are

$$\frac{f_s}{f_u + f_d} = 0.122 \pm 0.006, \qquad \frac{f_{\Lambda_b^0}}{f_u + f_d} = 0.259 \pm 0.018,$$

where the dominant sources of uncertainty are systematic and mainly due to external parameters. For $f_s/(f_u + f_d)$ the dominant systematic is the branching ratio of the decay $D_s^+ \to K^+ K^- \pi^+$ that gives a contribution of 3.3% to the systematic uncertainty. For $f_{\Lambda_b}/(f_u + f_d)$ the dominant uncertainty is due to the branching ratio of the $\Lambda_c^+ \to pK^+\pi^-$ decay, which gives a contribution of 5.3% to the total systematic.

The result obtained using 7 TeV data [25], $f_s/(f_u + f_d) = 0.1295 \pm 0.0075$, is consistent with the present result at 13 TeV. A recent LHCb measurement [24] studied the ratio f_s/f_u using the efficiency-corrected ratio (R) of yields between $B_s^0 \to J/\psi\phi$ and $B^+ \to J/\psi K^+$ decays. The result confirms a dependence of B_s^0 production on $p_T(H_b)$, but also shows a significant dependence of f_s/f_u with $\sqrt{s}$ as shown in Fig.7 (right). This requires further studies, in particular an analysis with semileptonic decays as presented here should be repeated with data at 7 and 8 TeV using all the updated analysis strategies and external inputs.

3.3 B_c^- production at $\sqrt{s} = 13\ TeV$

In this analysis, the B_c^- production fraction, f_c, is measured relative to the sum of B^0 and B^-, $f_d + f_u$, using a technique similar to the one used for B_s^0 and Λ_b^0 production. However, for the B_c^-, the inclusive semileptonic decay width is not equal to the other b-hadrons with light or strange quarks as in Eq.3.1, because both the b and c quarks can decay. Instead this analysis relies on the theoretical predictions of the branching fraction $\mathscr{B}(B_c^- \to J/\psi\mu^-\nu)$. The ratio $f_c/(f_u + f_d)$ is obtained as function of the transverse momentum of the B_c, and η.

The $B_c^- \to J/\psi\mu\nu$ events are selected from $J/\psi \to \mu^+\mu^-$ candidates with good vertex quality and a large flight distance from the PV. The other muon must be well identified and has to form a good vertex with the J/ψ. The variable used to extract the signal yields is the corrected mass defined as $m_{cor} = \sqrt{m(J/\psi\mu)^2 + p_\perp^2} + p_\perp$, where $p_\perp$ is the magnitude of the $J/\psi\mu$ momentum

transverse to the B_c^- candidate direction of flight. The variable m_{cor} is useful to suppress the contamination from $B_c^- \to J/\psi\tau^-\bar{\nu}_\tau(\tau^- \to \mu^-\nu_\tau\bar{\nu})$, $B_c^- \to \psi(2S)\mu^-\bar{\nu}$ and $B_c^- \to \chi_c\mu^-\bar{\nu}$ with the subsequent decay of the $\psi(2S)$ and χ_c into a J/ψ. The shape of m_{cor} for the 13 TeV data sample is shown in Fig. 8(left). There are about 4000 signal candidates in the 7 TeV sample and about 15000 in the 13 TeV sample.

The ratio $f_c/(f_u + f_d)$ can vary as function of p_T and η of the B_c, as observed in the Λ_b^0 and B_s^0 production. Hence the measurement is performed in bins of η and p_T. Because of the presence of the neutrino, the p_T is inferred using the k-factor as described in Section 3.2. The distribution of the ratio between the visible p_T and the true one in simulation is shown in Fig.8 (right).
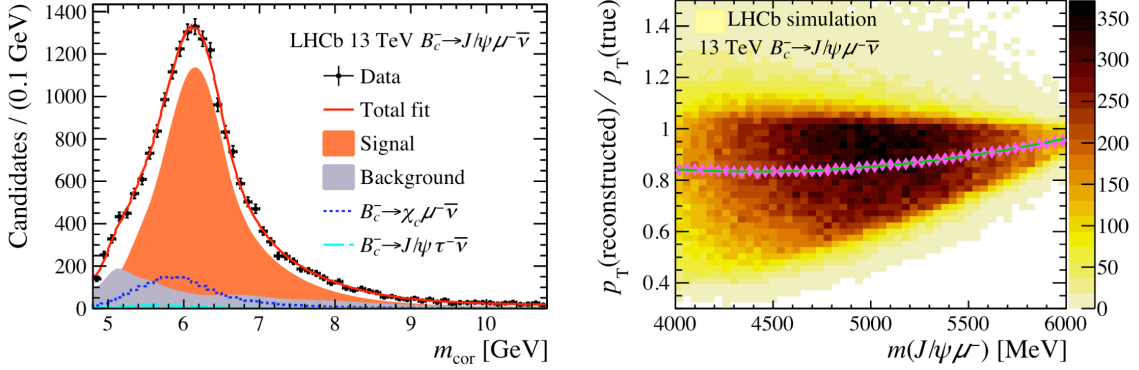
Figure 8: (Left) Fitted m_{cor} distributions in the 13 TeV sample. The signal and the backgrounds are shown as orange and grey areas. (Right) The k-factor corrections as a function of invariant mass of $m(J/\psi\mu)$ in simulation. The points (magenta) are the average k-factor corrections.

The ratio $f_c/(f_u + f_d)$ does not show significant dependence on pseudorapidity η in the range $2.5 < \eta < 4.5$, as can be seen in Fig.9(left). Instead $f_c/f_u + f_d$ clearly decreases as a function of $p_T(H_b)$. The slope of this dependence is similar to the one measured for the B_s^0 meson. The average production fraction times the $B_c \to J/\psi\mu\nu$ branching fraction, in the interval $4 < p_T(H_b) < 25$ GeV/c and for the 13 TeV sample, is

$$\frac{f_c}{f_u + f_d}\mathcal{B}(B_c^- \to J/\psi\mu\nu) = (7.36 \pm 0.08_{stat} \pm 0.30_{syst}) \times 10^{-5},$$

where the dominant source of systematic uncertainty is due to the shapes of the signal and background components used to fit the m_{cor} distribution, which are obtained from the simulation.

The predicted branching fraction of $\mathcal{B}(B_c^- \to J/\psi\mu\nu)$ available in the literature vary from 1.3% to 2.7% (see references in [8]). Using as the branching fraction an average value of 1.95%, the B_c^- production fraction ratio at 13 TeV is

$$\frac{f_c}{f_u + f_d} = (3.78 \pm 0.04_{stat} \pm 0.15_{syst} \pm 0.89_{BF}) \times 10^{-5},$$

where the third uncertainty, which is 24%, is due to the spread of the theoretical predictions of $\mathcal{B}(B_c^- \to J/\psi\mu\nu)$. The HPQCD collaboration provided a first prediction of the $B_c^- \to J/\psi\mu\nu$ decay width [26], which has an uncertainty of only 6.5%.

The first measurement of f_c summarized here, allows to extract the absolute branching fractions of the B_c^- meson decays.
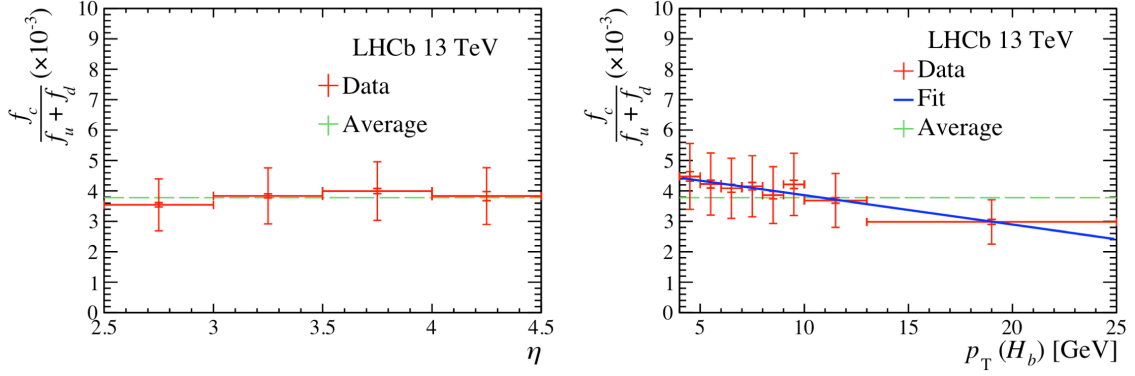
Figure 9: Ratio of production fractions as a function of η (left) and $p_T(H_b)$ (right) in 13 *TeV* data.

3.4 Ξ_b production at $\sqrt{s} = 7$, 8 and 13 *TeV*

Recently LHCb has made some first observations of specific decay modes of various *b*-baryons like Ξ_b^0, Ξ_b^+ and Ω_b^+ [27, 28, 29, 30]. However the absolute branching fractions cannot be accessed because there are no measurements of the $f_{\Xi_b^0}$, $f_{\Xi_b^-}$ and $f_{\Omega_b^-}$ fragmentation fractions. The same approach used to extract f_s/f_d could in principle be used to access f_{Ξ_b} using the semileptonic inclusive decays $\Xi_b^0 \to \Xi_c^+ \mu\nu X$ and $\Xi_b^- \to \Xi_c^0 \mu\nu X$. However the absolute branching fractions for the decays of Ξ_c^+ and Ξ_c^0 are not known well, so this approach is not feasible.

The alternative approach employed in this analysis, is to use the decays $\Lambda_b^0 \to J/\psi\Lambda$ and $\Xi_b^- \to J/\psi\Xi^-$, with $\Xi^- \to \Lambda\pi^-$. Charge-conjugate processes are implicitly included. These processes are related through $SU(3)$ flavor symmetry, $\Gamma(\Xi_b^-)/\Gamma(\Lambda_b^0) = 3/2$. The ratio R of the yields of $\Xi_b^- \to J/\psi\Xi^-$ and $\Lambda_b^0 \to J/\psi\Lambda$, corrected for the detection efficiency, is connected to $f_{\Xi_b^-}/f_{\Lambda_b^0}$ through

$$R = \frac{f_{\Xi_b^-}}{f_{\Lambda_b^0}} \frac{\mathscr{B}(\Xi_b^- \to J\psi\Xi^-)}{\mathscr{B}(\Lambda_b^0 \to J/\psi\Lambda)} = \frac{f_{\Xi_b^-}}{f_{\Lambda_b^0}} \frac{\mathscr{B}(\Xi_b^- \to J\psi\Xi^-)}{\mathscr{B}(\Lambda_b^0 \to J/\psi\Lambda)} \frac{\tau_{\Xi_b}}{\tau_{\Lambda_b}}, \tag{3.2}$$

which depends on the assumptions on the ratio of decay widths and the known ratio of lifetimes. The decays $\Xi_b^- \to J/\psi\Xi^-(\Xi^- \to \Lambda\pi^-)$ and $\Lambda_b^0 \to J/\psi\Lambda$ both have a J/ψ and a Λ in the final state, and have very similar kinematics. This feature allows strong cancellations in the detection systematic uncertainties. Because the Ξ^- and Λ have long lifetimes, most of the Λ from Ξ^- do not decay in the vertex detector and are reconstructed only from information from the trackers before and after the dipole magnet. To equalize the selection efficiencies, the Λ from Λ_b decays are also required to decay after the vertex detector. This reduces the yields of the reconstructed Λ_b, but allows a better control of the systematic uncertainties. Using data collected at $\sqrt{s} = 7$ and 8 *TeV* the ratio of production rate is $R = (10.8 \pm 0.9_{stat} \pm 0.8_{syst}) \times 10^{-2}$, and at $\sqrt{s} = 13$ *TeV* the ratio is $R = (13.1 \pm 1.1_{stat} \pm 1.0_{syst}) \times 10^{-2}$ where the uncertainties are statistical and experimental. The largest source of uncertainty is the assumption on the polarisations of the Λ_b and Ξ_b^- at production, and the detection efficiency of the π^- from the Ξ^- that enters directly into the ratio R. The results are obtained in the kinematic range $p_T < 20$ *GeV/c* and $2 < \eta < 6$. Assuming $SU(3)$ symmetry,

the ratio of fragmentation fractions at 13 *TeV* is

$$\frac{f_{\Xi_b^-}}{f_{\Lambda_b^0}} = (8.2 \pm 0.7_{stat} \pm 0.6_{syst} \pm 2.5_{SU(3)}) \times 10^{-2}, \tag{3.3}$$

which is consistent with the results at 7 and 8 *TeV* obtained in the same analysis, $f_{\Xi_b^-}/f_{\Lambda_b^0} = 6.7 \pm 0.5_{stat} \pm 0.5_{syst} \pm 2.0_{SU(3)}) \times 10^{-2}$. The last uncertainty of 30% is the typical size of $SU(3)$ breaking effects. These results are consistent with the predictions of [31]. To summarize, in the forward direction, assuming an equal production of Ξ_b^- and Ξ_b^0, the b-quark fragments into Ξ_b at a rate of about 15% of the rate of Λ_b production.

4. Conclusions

Several recent results on heavy flavour production in pp collisions have been reported. In general the differential cross-sections and the ratio of cross-sections at different centre of mass energies are described by predictions within uncertainties. But there are still inconsistencies that require further efforts from both theory and experiment. The precisions on f_s and $f_{\Lambda_b^0}$ production fractions have been greatly improved, this will allow precise measurements of absolute branching fractions of various decay modes. The presented measurement of f_c opens various opportunities with B_c decays. All the measurements presented provide important input for the tuning of simulations which are needed for precise evaluation of the detector acceptance of many decay processes, for all the LHC experiments.

References

[1] R. Aaij *et al.* [LHCb Collaboration], *Observation of J/ψp Resonances Consistent with Pentaquark States in $\Lambda_b^0 \to J/\psi K^- p$ Decays,* Phys. Rev. Lett. **115** (2015) 072001 doi:10.1103/PhysRevLett.115.072001 [arXiv:1507.03414 [hep-ex]].

[2] A. Alves, Jr. *et al.* [LHCb Collaboration], *The LHCb Detector at the LHC,* JINST **3** (2008), S08005 doi:10.1088/1748-0221/3/08/S08005

[3] R. Aaij *et al.* [LHCb Collaboration], *LHCb Detector Performance,* Int. J. Mod. Phys. A **30** (2015) no.07, 1530022 doi:10.1142/S0217751X15300227 [arXiv:1412.6352 [hep-ex]].

[4] R. Aaij *et al.* [LHCb Collaboration], *Measurement of ψ(2S) production cross-sections in proton-proton collisions at 7 and 13 TeV,* Eur. Phys. J. C **80** (2020) no.3, 185 doi:10.1140/epjc/s10052-020-7638-y [arXiv:1908.03099 [hep-ex]].

[5] R. Aaij *et al.* [LHCb Collaboration], *Measurement of the $\eta_c(1S)$ production cross-section in pp collisions at $\sqrt{s} = 13$ TeV,* Eur. Phys. J. C **80** (2020) no.3, 191 doi:10.1140/epjc/s10052-020-7733-0 [arXiv:1911.03326 [hep-ex]].

[6] R. Aaij *et al.* [LHCb Collaboration], *Measurement of Ξ_{cc}^{++} production in pp collisions at $\sqrt{s} = 13$ TeV,* Chin. Phys. C **44** (2020) no.2, 022001 doi:10.1088/1674-1137/44/2/022001 [arXiv:1910.11316 [hep-ex]].

[7] R. Aaij *et al.* [LHCb Collaboration], *Measurement of b hadron fractions in 13 TeV pp collisions,* Phys. Rev. D **100** (2019) no.3, 031102 doi:10.1103/PhysRevD.100.031102 [arXiv:1902.06794 [hep-ex]].

[8] R. Aaij *et al.* [LHCb Collaboration], *Measurement of the B_c^- meson production fraction and asymmetry in 7 and 13 TeV pp collisions,* Phys. Rev. D **100** (2019) no.11, 112006 doi:10.1103/PhysRevD.100.112006 [arXiv:1910.13404 [hep-ex]].

[9] R. Aaij *et al.* [LHCb Collaboration], *Measurement of the mass and production rate of Ξ_b^- baryons,* Phys. Rev. D **99** (2019) no.5, 052006 doi:10.1103/PhysRevD.99.052006 [arXiv:1901.07075 [hep-ex]].

[10] G. T. Bodwin, E. Braaten and G. P. Lepage, *Rigorous QCD analysis of inclusive annihilation and production of heavy quarkonium,* Phys. Rev. D **51** (1995) 1125 Erratum: [Phys. Rev. D **55** (1997) 5853] doi:10.1103/PhysRevD.55.5853, 10.1103/PhysRevD.51.1125 [hep-ph/9407339]. P. L. Cho and A. K. Leibovich, *Color octet quarkonia production,* Phys. Rev. D **53** (1996) 150 doi:10.1103/PhysRevD.53.150 [hep-ph/9505329].

[11] M. Cacciari, M. Greco and P. Nason, *The p_T spectrum in heavy flavor hadroproduction,* JHEP **9805** (1998) 007 doi:10.1088/1126-6708/1998/05/007 [hep-ph/9803400].

[12] R. Aaij *et al.* [LHCb Collaboration], *Measurement of forward J/ψ production cross-sections in pp collisions at $\sqrt{s} = 13$ TeV,* JHEP **1510** (2015) 172 Erratum: [JHEP **1705** (2017) 063] doi:10.1007/JHEP05(2017)063, 10.1007/JHEP10(2015)172 [arXiv:1509.00771 [hep-ex]].

[13] R. Aaij *et al.* [LHCb Collaboration], *Measurement of the $\eta_c(1S)$ production cross-section in proton-proton collisions via the decay $\eta_c(1S) \to p\bar{p}$,* Eur. Phys. J. C **75** (2015) no.7, 311 doi:10.1140/epjc/s10052-015-3502-x [arXiv:1409.3612 [hep-ex]].

[14] Y. Feng, J. He, J. P. Lansberg, H. S. Shao, A. Usachov and H. F. Zhang, *Phenomenological NLO analysis of η_c production at the LHC in the collider and fixed-target modes,* Nucl. Phys. B **945** (2019) 114662 doi:10.1016/j.nuclphysb.2019.114662 [arXiv:1901.09766 [hep-ph]].

[15] M. Butenschoen, Z. G. He and B. A. Kniehl, *η_c production at the LHC challenges nonrelativistic-QCD factorization,* Phys. Rev. Lett. **114** (2015) no.9, 092004 doi:10.1103/PhysRevLett.114.092004 [arXiv:1411.5287 [hep-ph]].

[16] H. Han, Y. Q. Ma, C. Meng, H. S. Shao and K. T. Chao, *η_c production at LHC and indications on the understanding of J/ψ production,* Phys. Rev. Lett. **114** (2015) no.9, 092005 doi:10.1103/PhysRevLett.114.092005 [arXiv:1411.7350 [hep-ph]].

[17] H. F. Zhang, Z. Sun, W. L. Sang and R. Li, *Impact of η_c hadroproduction data on charmonium production and polarization within NRQCD framework,* Phys. Rev. Lett. **114** (2015) no.9, 092006 doi:10.1103/PhysRevLett.114.092006 [arXiv:1412.0508 [hep-ph]].

[18] R. Aaij *et al.* [LHCb Collaboration], *Observation of the doubly charmed baryon Ξ_{cc}^{++},* Phys. Rev. Lett. **119** (2017) no.11, 112001 doi:10.1103/PhysRevLett.119.112001 [arXiv:1707.01621 [hep-ex]].

[19] R. Aaij *et al.* [LHCb Collaboration], *Measurement of the Lifetime of the Doubly Charmed Baryon Ξ_{cc}^{++},* Phys. Rev. Lett. **121** (2018) no.5, 052002 doi:10.1103/PhysRevLett.121.052002 [arXiv:1806.02744 [hep-ex]].

[20] I. I. Bigi, T. Mannel and N. Uraltsev, *Semileptonic width ratios among beauty hadrons,* JHEP **1109** (2011) 012 doi:10.1007/JHEP09(2011)012 [arXiv:1105.4574 [hep-ph]].

[21] M. Tanabashi *et al.* [Particle Data Group], *Review of Particle Physics* Phys. Rev. D **98** (2018) no.3, 030001. doi:10.1103/PhysRevD.98.030001

[22] R. Aaij *et al.* [LHCb Collaboration], *Measurement of b-hadron production fractions in 7 TeV pp collisions,* Phys. Rev. D **85** (2012), 032008 doi:10.1103/PhysRevD.85.032008 [arXiv:1111.2357 [hep-ex]].

[23] R. Aaij *et al.* [LHCb Collaboration], *Study of the kinematic dependences of Λ_b^0 production in pp collisions and a measurement of the $\Lambda_b^0 \to \Lambda_c^+ \pi^-$ branching fraction,* JHEP **08** (2014), 143 doi:10.1007/JHEP08(2014)143 [arXiv:1405.6842 [hep-ex]].

[24] R. Aaij *et al.* [LHCb], *Measurement of f_s/f_u variation with proton-proton collision energy and B-meson kinematics,* Phys. Rev. Lett. **124** (2020) no.12, 122002 doi:10.1103/PhysRevLett.124.122002 [arXiv:1910.09934 [hep-ex]].

[25] R. Aaij *et al.* [LHCb Collaboration], *Measurement of the fragmentation fraction ratio f_s/f_d and its dependence on B meson kinematics,* JHEP **1304** (2013) 001 doi:10.1007/JHEP04(2013)001 [arXiv:1301.5286 [hep-ex]]; f_s/f_d value updated in LHCb-CONF-2013-011.

[26] J. Harrison, $B_c \to J/\psi$ *Form Factors and $R(J/\psi)$ using Lattice QCD*, preliminary results at this conference.

[27] R. Aaij *et al.* [LHCb Collaboration], *Studies of beauty baryon decays to $D^0 ph^-$ and $\Lambda_c^+ h^-$ final states,* Phys. Rev. D **89** (2014) no.3, 032001 doi:10.1103/PhysRevD.89.032001 [arXiv:1311.4823 [hep-ex]].

[28] R. Aaij *et al.* [LHCb Collaboration], *Evidence for the strangeness-changing weak decay $\Xi_b^- \to \Lambda_b^0 \pi^-$,* Phys. Rev. Lett. **115** (2015) no.24, 241801 doi:10.1103/PhysRevLett.115.241801 [arXiv:1510.03829 [hep-ex]].

[29] R. Aaij *et al.* [LHCb Collaboration], *Precision measurement of the mass and lifetime of the Ξ_b^0 baryon,* Phys. Rev. Lett. **113** (2014), 032001 doi:10.1103/PhysRevLett.113.032001 [arXiv:1405.7223 [hep-ex]].

[30] R. Aaij *et al.* [LHCb Collaboration], *Observation of the $\Xi_b^- \to J/\psi \Lambda K^-$ decay,* Phys. Lett. B **772** (2017), 265-273 doi:10.1016/j.physletb.2017.06.045 [arXiv:1701.05274 [hep-ex]].

[31] H. Y. Jiang and F. S. Yu, *Fragmentation-fraction ratio f_{Ξ_b}/f_{Λ_b} in b- and c-baryon decays,* Eur. Phys. J. C **78** (2018) no.3, 224 doi:10.1140/epjc/s10052-018-5704-5 [arXiv:1802.02948 [hep-ph]].

PoS(Beauty2019)025